Long-term Satellite-derived Bathymetry of Arctic Supraglacial Lake from ICESat-2 and Sentinel-2

Jinhao Lv [1], Shaoyu Li[1, 3], Xiaoming Wang[2], Chao Qi [1, 3, *], Meng Zhang[1, 3]

[1] College of Geodesy and Geomatics, Shandong University of Science and Technology, Qingdao, China – (qichoice007, skd_zhangmeng)@sdust.edu.cn, (lvjinhao2003, lishaoyu054)@163.com
[2] CCCG Xingyu Technology Co., Ltd, Beijing, China - sdust_wxm@163.com
[3] Key Laboratory of Ocean Geomatics, Ministry of Natural Resources of China, Qingdao 266590, China – (qichoice007, skd_zhangmeng)@sdust.edu.cn, lishaoyu054@163.com

Keywords: Arctic Supraglacial Lake, Satellite-derived Bathymetry, Long-term detection, Sentinel-2, ICESat-2

Abstract

The polar ice sheets serve as natural thermostats, regulating Earth’s temperatures. The Greenland Ice Sheet (GrIS), the second-largest ice sheet, is a critical indicator of climate change and global warming. Estimating the volume of supraglacial lakes on the GrIS, which is directly linked to the extent of melting in the Arctic ice sheet, requires information on both lake area and water depth. Conventional bathymetric methods (i.e., airborne bathymetric LiDAR, shipborne echo-sounder) are commonly used for accurate water depth measurement. However, polar supraglacial lakes face challenging conditions, leading to uncertainties in their spatial and temporal distribution. To overcome the limitations, this study combines Sentinel-2 and ICESat-2 (Ice, Cloud, and Land Elevation Satellite-2) to estimate bathymetry and detect changes in lake volume on the GrIS from 2019 to 2023. Firstly, Sentinel-2 images were pre-processed, and ICESat-2 single-photon LiDAR points were extracted using the DBSCAN (Density-Based Spatial Clustering of Applications with Noise) method, followed by the bathymetric corrections as the training data. Subsequently, three bathymetry models (i.e., log-linear, log-ratio, and BP (Back Propagation) neural network) were constructed using Sentinel-2 images and ICESat-2 data. Lastly, the high-resolution ArcticDEM (Arctic Digital Elevation Model) was used as the validation data to assess the satellite-derived bathymetry accuracy. In this study, the log-ratio model yielded the best results with the R^2, RMSE, and MAE of 0.92, 0.79 m (lower than 10% of the maximum depth), and 0.62 m. The results demonstrate the feasibility of the integrated active and passive remote sensing approach for bathymetry in Arctic supraglacial lakes.

1. Introduction

The melting of glaciers in the Arctic has significant implications for global climate change and is a key manifestation of global warming. Arctic glaciers are considered natural thermostats, and changes in the volume of Arctic supraglacial lakes can provide a direct indication of the extent of Arctic glacier melting (Box et al., 2022). Estimating water depth is crucial for detecting the volume of Arctic lakes. Conventional bathymetry methods, such as airborne LiDAR and shipborne echo-sounder are well-developed and can obtain accurate water depth data (ZHAO et al., 2001). However, they have limitations in remote or sensitive areas in terms of time and space (Li et al., 2022). Arctic lakes are often located in inland areas with harsh climates, making it difficult for ship-based platforms to access them. Additionally, for some sensitive areas, airborne bathymetric methods (e. g. LiDAR) are restricted. In general, these conventional methods have limitations in remote and harsh regions, and are both time-consuming and costly.

Satellite-derived Bathymetry (SDB) is emerging as a pivotal technology for large-scale shallow water bathymetry, leveraging ocean optics to estimate coastal water depth. (Albright., et al.2020; Duplančić Leder., 2019; Thomas et al. 2021). It addresses the temporal and spatial limitations of conventional bathymetry methods by using high-temporal-resolution satellite data. In 2018, NASA launched ICESat-2 (Ice, Cloud, and Land Elevation Satellite-2), intending to provide a global distribution of elevation measurements. To ensure the accuracy of bathymetric inversion, the detected underwater photons of ICESat-2 were used as *in-situ* measurement data in many studies (Zhang et al., 2022; Li et al., 2023). Therefore, using both passive and active remote sensing datasets is feasible for SDB.

Ma et al. (Ma et al., 2021) used Sentinel-2 and ICESat-2 to estimate bathymetry in the Xisha Islands of the South China Sea and the south-eastern islands of the Bahamas. Le Quilleuc et al. (Le Quilleuc et al., 2021) used very high-resolution Pleiades-1 imagery and ICESat-2 data for bathymetric inversion and generation of benthic habitats maps using maximum likelihood supervised classification. Moreover, machine learning models have been integrated into SDB. Guo et al. (Guo et al., 2022) used a BP (Back Propagation) neural network within the SDB framework to derive water depths in the Virgin Islands of the eastern Caribbean Sea and the West of Oahu Island, achieving higher accuracy than the conventional bathymetric models. He et al. (He et al., 2024) analyzed water depth changes before and after earthquakes in Huohua Lake which is located at Jiuzhai Valley nature reserve with WorldView-2 (WV-2) and three machine learning models (i.e., random forest (RF), support vector machine (SVM), and multilayer perceptron (MLP) models). Furthermore, there are many studies for bathymetric inversion research in polar regions. Zheng et al. (Zheng et al., 2012) used Landsat-5 and multibeam bathymetric data to estimate the water depths of polar lakes in the northern coastal ice fields of Alaska. Fitzpatrick et al., (Fitzpatrick et al., 2014) used MODIS imagery and the field-measured bathymetric data to detect the volume changes of the Greenland Ice Sheet (GrIS) lakes over a decade. Moussavi et al. (Moussavi et al. 2016) used stereoscopic measurement techniques with WV-2 imagery to acquire Digital Depth Models (DDMs) of GrIS supraglacial lakes. Fricker et al., (Fricker et al., 2021) combined ICESat-2 data with Sentinel-2 and Landsat-8 imagery to estimate water depths in polar melt

* Corresponding author

regions. These studies demonstrate that remote sensing datasets can be utilized to derive bathymetry in polar areas, enabling cost-effective detection of water depth and quantification of stored meltwater volumes in the extreme climate of the Arctic region.

However, utilizing airborne bathymetric LiDAR, shipborne sonar, or GNSS-RTK (Global Navigation Satellite System- Real-Time Kinematic) as *in-situ* data for bathymetry inversion in polar regions needs huge costs and labour. The water depth derived through conventional methods is subject has various limitations and is difficult for long-term water depth detection requirements. Therefore, this study used both passive and active remote sensing datasets (i.e., Sentinel-2 and ICESat-2) to derive bathymetry on the southwest region of the GrIS and detect lake volume changes over five years from 2019 to 2023. Initially, ICESat-2 signal photons were extracted using the DBSCAN (Density-Based Spatial Clustering of Applications with Noise) method and then processed with refraction correction to obtain water depth. Sentinel-2 imagery was pre-processed with radiometric correction and atmospheric correction, then the supraglacial lakes were extracted from the images. Secondly, underwater signal photons extracted from ICESat-2 were geographically matched with remote sensing reflectance data from the Sentinel-2. In this study, three different models: the log-linear model (Lyzenga, 1978; Lyzenga, 1985), the log-ratio model (Stumpf et al., 2003), and the BP neural network model were used to derive bathymetry in southwest GrIS supraglacial lakes. The accuracy of bathymetry was validated using high-resolution ArcticDEM (Arctic Digital Elevation Model) data. Finally, the bathymetric maps were produced based on the model with the best accuracy and efficiency for long-term bathymetry in this study. The proposed method enables the detection of changes in the volume of supraglacial lakes in the Arctic, which reflects the extent of melting in the GrIS. This method can also provide a valuable reference for detecting Arctic climate changes.

2. Study Area and Data

2.1 Study Area

The largest ice sheet in the Arctic is located on Greenland Island, with 80% of its area covered by ice sheets. It is the world's second-largest ice sheet, surpassed only by the Antarctic ice sheet. However, the GrIS is more vulnerable than the Antarctic ice sheet and highly sensitive to climate warming. Consequently, the melting of the GrIS serves as a significant indicator of global climate change. This study focuses on the southwest region of the GrIS, where there are a large number of supraglacial lakes (Figure 1). The water quality of the supraglacial lakes is clear, making it feasible to extract ICESat-2 underwater photons and providing favorable conditions for SDB. The ArcticDEM offers a high spatial resolution and numerous empty lake basins that can be utilized to validate the precision of the bathymetry results.

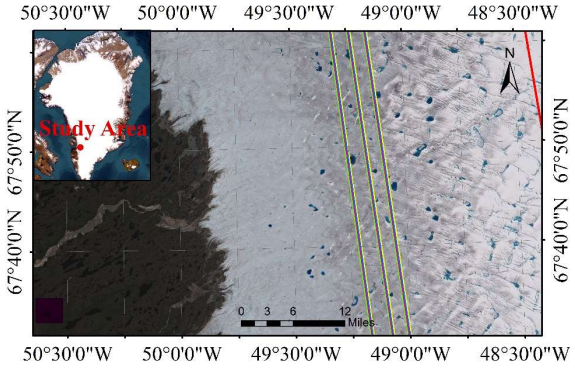

Figure 1. The study area is a part of the southwest of GrIS, which has a relatively dense distribution of supraglacial lakes compared to other regions. The base map is a Sentinel-2 imagery on 2022/07/17 and Earthstar Geographics via ESRI. The red line corresponds to the ICESat-2 track on 2019/07/16, the green lines correspond to the ICESat-2 track on 2020/07/17, the pink lines correspond to the ICESat-2 track on 2021/07/15, the blue lines correspond to the ICESat-2 track on 2022/07/14, the yellow lines correspond to the ICESat-2 track on 2023/07/12.

2.2 Sentinel-2 Satellite Imagery

The Sentinel-2 imagery is available for free from the European Space Agency's (ESA) Copernicus Data hub, consisting of Sentinel-2A and Sentinel-2B. Each satellite is equipped with the same Multi-Spectral Instrument (MSI), capable of capturing imagery in 13 spectral bands, including visible, NIR (Near-infrared), and SWIR (Shortwave infrared). The Copernicus Data Hub provides two levels of data products: L1C (Level-1C) and L2A (Level-2A). L1C products are atmospheric reflectance products that have been ortho-rectified and geometrically corrected at the sub-pixel level, while L2A products primarily contain atmospherically corrected bottom-of-atmosphere reflectance data. Both L1C and L2A data were used in this study. L1C was corrected with atmospheric correction using the Sen2Cor (version 2.11) into L2A. This study used Band 2 (Blue), Band 3 (Green), Band 4 (Red), and Band 8 (Near infrared) with a spatial resolution of 10 m. The SNAP software was used to process the Sentinel-2 data in this study. The information on the selected images for the study areas is listed in Table 1.

Year	Dataset	Date
2019	Sentinel-2	2019/07/16
	ICESat-2	2019/07/16
2020	Sentinel-2	2020/07/17
	ICESat-2	2020/07/17
2021	Sentinel-2	2021/07/17
	ICESat-2	2021/07/15
2022	Sentinel-2	2022/07/17
	ICESat-2	2022/07/14
2023	Sentinel-2	2023/07/12
	ICESat-2	2023/07/12

Table 1. Details information on the acquisition dates of Sentinel-2 and ICESat-2 data for bathymetric mapping.

2.3 ICESat-2 LiDAR Data

ICESat-2 satellite, equipped with the Advanced Topographic Laser Altimeter System (ATLAS), was launched by NASA on September 15, 2018, marking the inception of a new generation of global altimetry satellites. Its mission is to provide high-precision elevation measurements for polar ice sheets, sea ice, and forest vegetation, playing an irreplaceable role in polar ice and snow remote sensing applications (Xie et al., 2020). ICESat-2 introduces single photon detection technology for the first time, significantly improving the data acquisition rate for terrain detection (Liu et al., 2022). The data is referenced to the WGS84 ellipsoid, and the payload is designed with 6 beams. These beams have a laser repetition rate of up to 10 kHz, a footprint size of 17 m, and a footprint spacing of 0.7 m. This configuration allows for

the continuous detection of six tracks under the satellite. Among the six beams of ATLAS, three beams have stronger energy, while the other three beams have weaker energy. This enables the measurement target to have different reflections and reduces problems caused by excessive photon counts in surface reflectance inversion. In this study, ICESat-2 Level-2 ATL03 data were used to construct the bathymetric inversion model, which includes height, latitude, longitude, and time information of each photon transmitted by the ATLAS instrument on board the satellite. The raw ATL03 data contains a large number of noise photons. Although the ATL03 product provides a method to label noise photons based on confidence parameters, it suffers from a serious misclassification issue. In this study, the DBSCAN method is used to extract bathymetric photons and perform refraction correction on the extracted underwater bathymetric photons.

2.4 ArcticDEM

The ArcticDEM data used in the study was obtained from the Polar Geospatial Center at the University of Minnesota. ArcticDEM covers the entire area above 60°N latitude and provides high-resolution DEM. ArcticDEM utilizes satellite stereo imaging principles, combined with stereo imagery from WorldView-1, 2, 3, and a small number of GeoEye-1 satellites. It employs Surface Extraction with TIN-based Search-space Minimization (SETSM) software to generate DEM data with a spatial resolution of up to 2 m (Morin et al., 2016). The emergence of ArcticDEM is of great significance for understanding Arctic terrain and climate change. In the ArcticDEM data, empty basins corresponding to the supraglacial lakes of the GrIS can be identified, enabling the extraction of elevation data for the lake floor. The construction of ArcticDEM took a considerable amount of time, making it challenging to synchronize with Sentinel-2 imagery and ICESat-2 data in terms of timing. Previous research (Melling et al., 2023) indicated that there may be fluctuations in water depth between the acquisition times of ArcticDEM data and Sentinel-2 and ICESat-2. However, it is unlikely that the underlying bedrock topography of the supraglacial lakes would significantly change within a short period. By delineating the boundaries of the supraglacial lakes using Sentinel-2 imagery and ICESat-2 data, and vertically aligning the elevation of the edge photons on the surface of the ICESat-2 lake with the ArcticDEM hollow lake basin, the water depth can be derived from ArcticDEM. The water depths derived from ArcticDEM are basically consistent with ICESat-2 elevation data, demonstrating the viability of using ArcticDEM as validation data for bathymetric inversion. The acquisition date of ArcticDEM data used in this study is 2019/09/24.

3. Method

3.1 Extraction of water areas

To extract the supraglacial lakes, it is necessary to separate the water from the ice sheet within the study area. In this study, the strong contrast in reflectance between water bodies in the green and near-infrared bands was used to construct the Normalized Difference Water Index (NDWI) (McFeeters, 1996), expressed as Eq. (1). By selecting appropriate thresholds, the supraglacial lakes can be extracted from the GrIS. To ensure the representativeness of the selected study area, this study only used lakes with a water surface area larger than 200,000 m^2 for bathymetric analysis.

$$NDWI = \frac{(Green - NIR)}{(Green + NIR)} \tag{1}$$

where $Green$ = reflectance at the green band
NIR = reflectance at the near-infrared band

3.2 Detection of ICESat-2 Lake-floor Photons

In the raw data of ATL03, there are a large number of noise photons due to the solar background. Due to this reason, the data cannot be directly utilized and requires the removal of noise photons to extract signal photons for bathymetry. This study utilized the DBSCAN algorithm to segment signal photons and noise photons into different clusters by adjusting the threshold of *MinPts*, thereby achieving the goal of extracting signal photons while eliminating noise photons. The calculation for the adaptive threshold *MinPts* is as Eq. (2) (Ma et al., 2021):

$$MinPts = \frac{2SN_1 - SN_2}{\ln\left(\frac{2SN_1}{SN_2}\right)} \tag{2}$$

where SN_1 = number of signal photons
SN_2 = number of noise photons

3.3 Bathymetric Correction of Lake-floor Photons

Since the original ATL03 data did not take into account the refraction caused by the change of laser propagation medium, the detected underwater signal photon height is lower than the actual signal photon height (Figure 2). Therefore, it is necessary to perform refraction correction for horizontal and vertical offsets caused by the different refractive indices of air and water. Due to the relatively calm surface of supraglacial lakes, the influence of water surface fluctuations and tides on water depth was neglected in this study. After processing, these underwater signal photons can be used to obtain the water depth of supraglacial lakes. Figure 2 shows the refraction correction of ICESat-2 data. The equation for water depth refraction correction can be expressed as Eq. (3) (Parrish et al., 2019):

$$D = \left\{1 - \tan\left[\frac{(\theta_1 - \theta_2)}{2}\right]\sin(\theta_1 - \theta_2)\right\} R_c \tag{3}$$

where D = corrected water depth
θ_1 = incidence angle to the water surface
θ_2 = refraction angle in the water column
R_c = corrected laser range

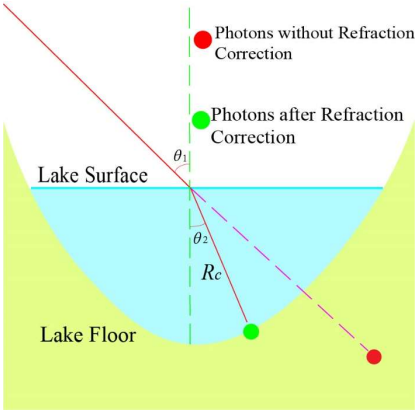

Figure 2. Illustration of ICESat-2 laser refraction correction.

3.4 SDB Methods with Sentinel-2 and ICESat-2 Data

The linear bathymetric inversion model based on logarithmic transformation was proposed by Lyzenga (Lyzenga, 1978; Lyzenga, 1985), which uses a combination of multi-band reflectance to derive bathymetry. The equation is expressed as Eq. (4).

$$Z = a_0 + \sum_{i=1}^{N} a_i \ln\left[L(\lambda_i) - L_\infty(\lambda_i)\right] \quad (4)$$

where Z = water depth, a_0 and a_i are parameters

$L(\lambda_i)$ = subsurface bottom reflectance of the i-th band

$L_\infty(\lambda_i)$ = reflectance in deeper water areas of the i-th band

The bathymetric inversion model based on logarithmic ratio was proposed by Stumpf et al. (Stumpf et al., 2003) which establishes a linear regression relationship between band ratio and prior water depth using the reflectance of the blue and green bands. The equation is expressed as Eq. (5).

$$Z = m_1 \frac{\ln\left(nR_\omega(\lambda_i)\right)}{\ln\left(nR_\omega(\lambda_j)\right)} + m_0 \quad (5)$$

where Z = water depth

m_0, m_1, and n = parameters

$R_\omega(\lambda_i)$ = reflectance of the i-th band

The BP neural network is the most widely used neural network in current applications, capable of mapping complex nonlinear relationships (Bin et al., 2016; Guo et al., 2022). Generally, the BP neural network consists of an input layer, a hidden layer(s), and an output layer, each containing several nodes. The principle of the BP neural network is to perform forward propagation by inputting the depth measurement data of ICESat-2 signal photons into the spectral reflectance data of Sentinel-2 through the input layer. After processing through the hidden layer, the data is transmitted to the output layer to predict water depth. If the output water depth result has a large error, error backpropagation is performed. By continuously iterating and adjusting the weights of each layer's nodes, the error can be reduced to a satisfactory level. In this study, the input layer consists of 3 nodes corresponding to the reflectance of red, green, and blue bands in Sentinel-2 images, the hidden layer consists of 11 nodes, and the output layer consists of 1 node. The activation function is Sigmoid, and the training function is Trainlm.

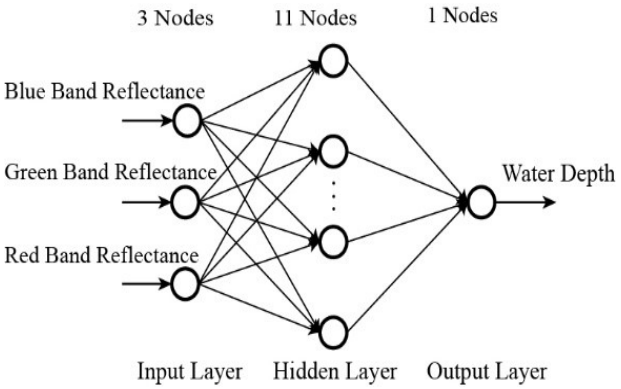

Figure 3. The structure of the BP neural network in this study.

4. Results

4.1 Results of ICESat-2 Bathymetry

In the southwest of Greenland, there are numerous supraglacial lakes. Figure 4 (a) shows one sample lake extraction result of the Sentinel-2 image on 2022/07/17. The Sentinel-2 data exhibits good quality and low cloud cover in the study area, which has minimal impact on the bathymetric inversion. Figure 4 (b) and (c) show the signal photon extraction and refraction correction results of one sample ICESat-2 data track on 2022/07/14. Although the ICESat-2 data contains considerable noise photons, the outline of the GrIS remains clearly visible, allowing us to identify the photons of the lake surface and lake bottom. The ICESat-2 photon data underwent processing, including noise filtering and the removal of elevation outliers along the supraglacial lake tracks, both excessively high and low in latitude. Subsequently, the DBSCAN algorithm was applied to the filtered data to extract photons of the lake surface and lake bottom (Figure 4 (b)). The x-axis represents the latitude of the ICESat-2 laser trajectory, and the y-axis represents the elevation of the GrIS. Then, the refraction correction was performed on the extracted photons from the lake bottom to obtain the underwater bathymetric photons, which were used to construct the bathymetric inversion models (Figure 4 (c)).

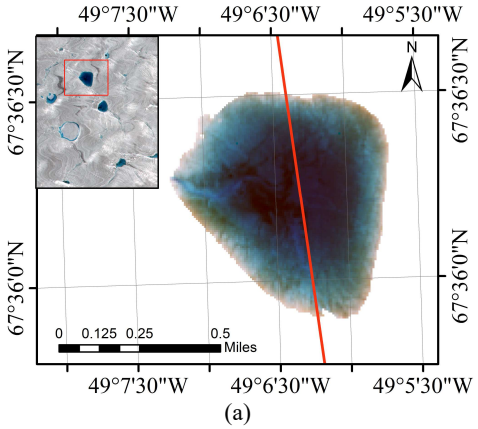

(a)

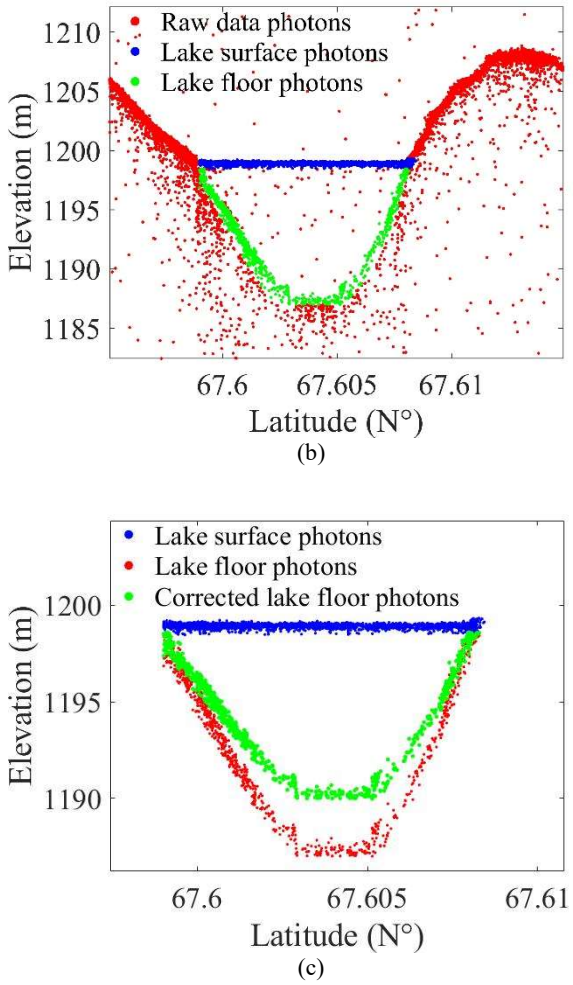

Figure 4. Examples of supraglacial lake extraction and ICESat-2 data processing. (a) The Sentinel-2 image of the lake on 2022/07/17. The red line represents a laser trajectory of ICESat-2 ATL03 data. (b) The bathymetric photons extraction result of one sample ICESat-2 track on 2022/07/14, where red points represent raw data containing noise photons; blue points represent lake surface photons; green points represent lake floor photons extracted by DBSCAN. (c) The refraction correction result of the ICESat-2 lake floor signal photons, where blue points represent surface photons, red points represent lake floor photons before refraction correction and green points represent the corrected lake floor photons.

4.2 Results of SDB using Sentinel-2 and ICESat-2

The log-linear model, the log-ratio model, and the BP neural network model were used to perform bathymetry on the Sentinel-2 and ICESat-2 data in July 2020. The accuracy was validated with points selected from the corresponding lakes in the ArcticDEM, as shown in Figure 5. It was observed that the inversion accuracy of the log-linear model was relatively low with R^2, RMSE and MAE of 0.79, 1.15 m and 0.89 m, respectively. (Figure 5 (a)). Meanwhile, the accuracy of both the log-ratio model and the BP neural network model was relatively good (Figure 5 (b) and (c)). The R^2, RMSE and MAE were 0.92, 0.79 m and 0.62 m for the log-ratio model, and the R^2, RMSE and MAE were 0.86, 0.87 m and 0.64 m for the BP model. Table 2 shows the accuracy evaluation of the three models. However, due to the limited availability of sufficient ICESat-2 underwater depth photons as training data, the BP neural network exhibited relatively large errors in certain regions. Additionally, considering the large areas for bathymetry, the efficiency of the BP neural network model was relatively low. Compared to the other two models, the log-ratio model yielded the best accuracy and efficiency with the R^2 of 0.92, RMSE of 0.79 m and MAE of 0.62 m. Therefore, it was adopted for producing the final bathymetric maps.

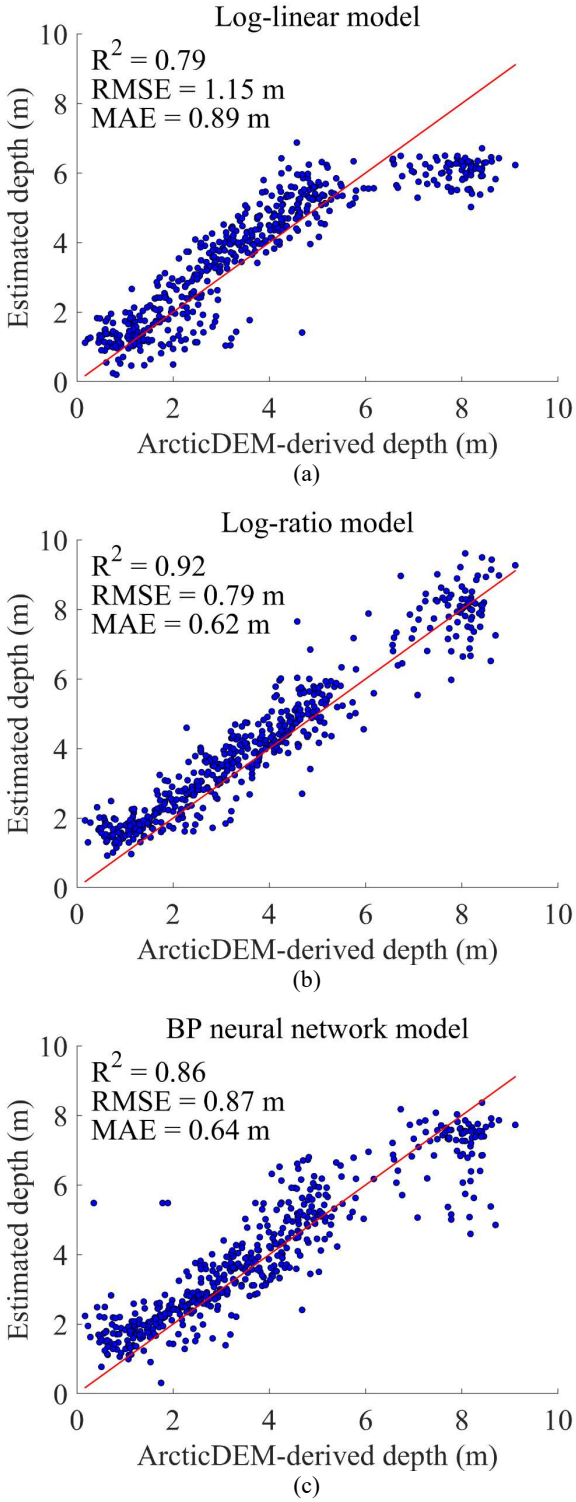

Figure 5. Validation results of three bathymetric models. (a) The log-linear model. (b) The log-ratio model. (c) The BP neural network model. The red line is the 1:1 line.

Models	R^2	RMSE (m)	MAE (m)
log-linear model	0.79	1.15	0.89
log-ratio model	**0.92**	**0.79**	**0.62**
BP neural network	0.86	0.87	0.64

Table 2. Accuracy evaluation of the three models.

This study produced bathymetric maps with the log-ratio model of supraglacial lakes in the southwest of GrIS over five years from 2019 to 2023, as shown in Figure 6 (a)-(e), respectively. Due to the issue of overestimation or underestimation of water depth caused by anomalous pixel values during the inversion process, we manually removed these values based on data statistics. This ensured that the lake depth fell within a normal range. The above operations were conducted using ENVI software (version 5.3.1).

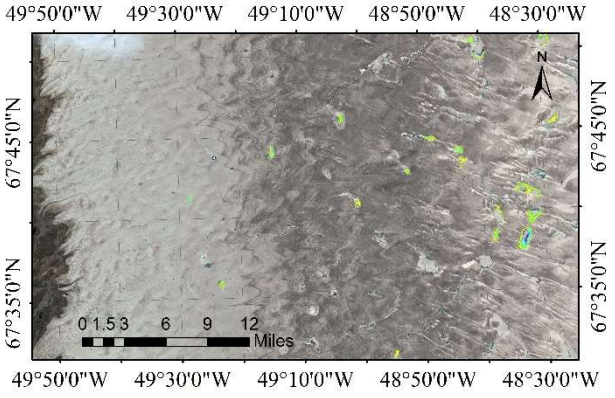

(a)

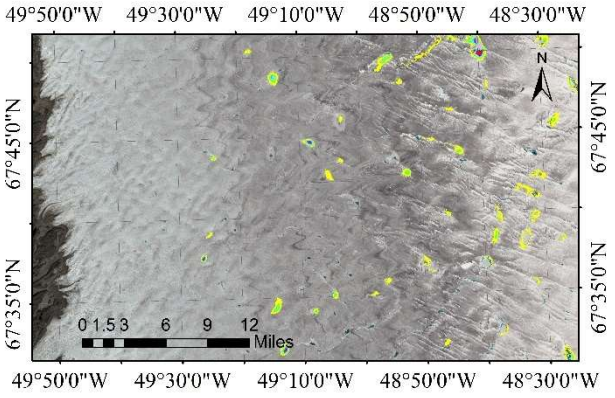

(b)

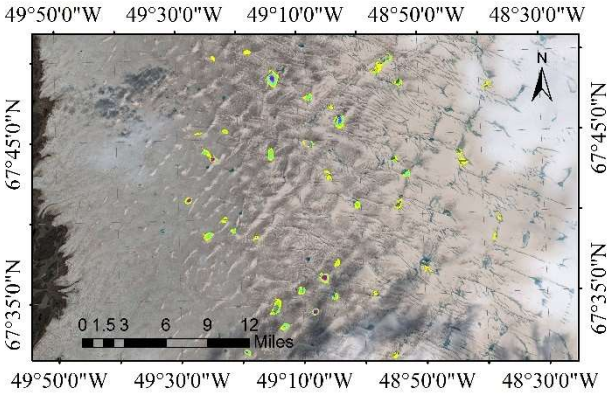

(c)

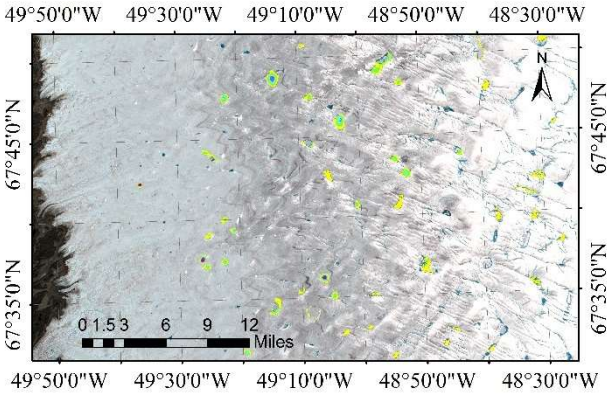

(d)

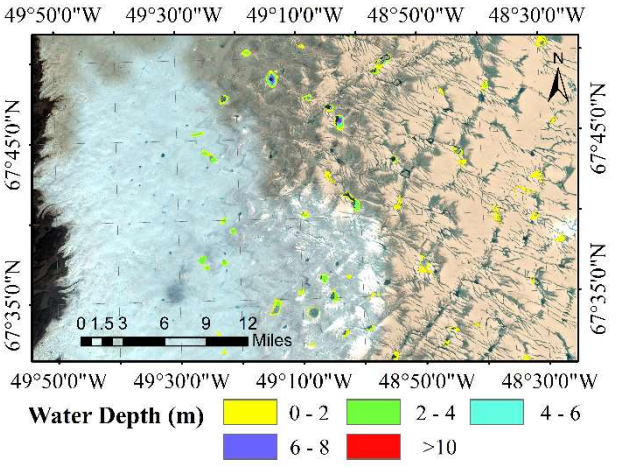

(e)

Figure 6. Bathymetry maps of supraglacial lakes in the southwest of GrIS from 2019 to 2023. (a) 2019, (b) 2020, (c) 2021, (d) 2022, and (e) 2023.

It is clear from the images that the distribution of the lake in mid-July 2019 was relatively small compared to other years in the same period, and the number of lakes remained stable in subsequent years. The bathymetric maps revealed that the majority of water depths derived from the bathymetric inversion model for Arctic supraglacial lakes in this study area were below 10 m.

5. Discussion

5.1 Differences and Analysis of Bathymetry Models

This study used three SDB models: log-linear model, log-ratio model, and BP neural network model. The linear model can incorporate multiple bands to construct the model, achieving high accuracy in shallow water areas. However, the accuracy decreases in deep-water areas. Moreover, there is no guarantee that the reflectivity of the deep-water band is less than that of the underground bottom, resulting in a negative difference between the two. During model training, the BP neural network achieved acceptable accuracy when compared with ArcticDEM. However, the construction and inversion process of the BP neural network model was relatively slow, resulting in longer processing times. Furthermore, in areas lacking training data, the BP neural network was unable to accurately define the relationship between reflectance and water depth. The log-ratio model achieved satisfactory accuracy in the bathymetry process, with higher efficiency than the BP neural network. Therefore, the log-ratio model was selected to produce bathymetric maps in this manuscript.

5.2 Analysis of Lake Volume Changes

Considering the various factors influencing polar temperatures, the time when the lakes reach their peak volume varies each year. Therefore, it is challenging to accurately extract data corresponding to the peak volume for each year for SDB. Instead, the approximate times were chosen for water depth inversion of each year to study the pattern of changes in water depth of polar supraglacial lakes. Figure 7 (a) and (b) show the morphology and the bathymetry of one supraglacial lake in 2019 and 2022, respectively. Meanwhile, to visually represent the changes in the volume of supraglacial lakes more intuitively, the obtained water depth results were multiplied by the pixel size and then summed to obtain the volume of supraglacial lakes in the study area, as shown in Eq. (6). The volume calculation results of supraglacial lakes from 2019 to 2023 are shown in Figure 8. It should be noted that the spatial resolution of Sentinel-2 imagery is 10 m here.

$$V = \sum_{i=1}^{n} (Z_i * S) \tag{6}$$

where V = lake volume
Z_i = water depth of the i-th pixel
S = pixel size
n = total number of pixels

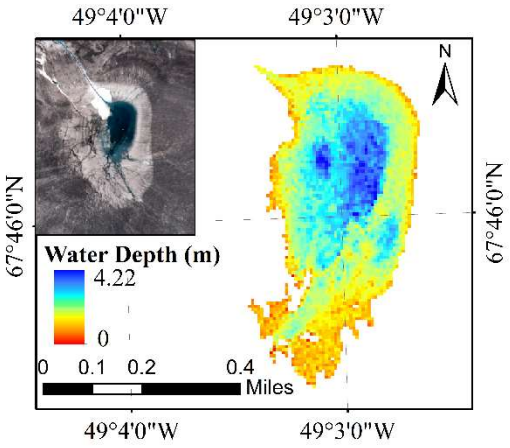

(a)

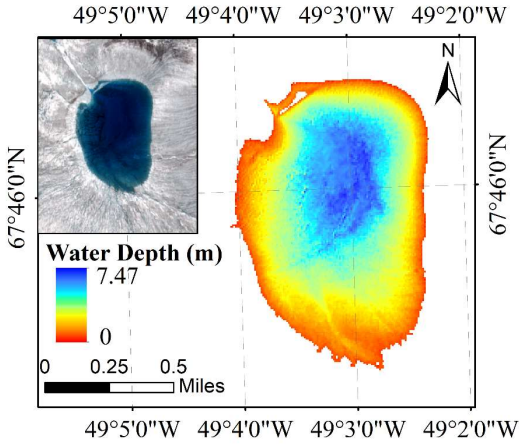

(b)

Figure 7. The morphology and bathymetry of the same supraglacial lake in 2019 and 2022. (a) The bathymetric map retrieved from Sentinel-2 on 2019/07/16. (b) The bathymetric map retrieved from Sentinel-2 on 2022/07/17.

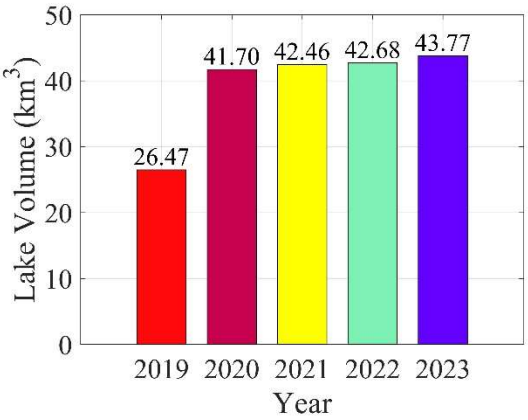

Figure 8. Lake Volume changes from 2019 to 2023

By combining Sentinel-2 imagery with SDB inversion results, it can be observed that in 2019, both the number of lakes and their depths were significantly lower compared to subsequent years (Figure 6 (a)), while the water depth remained relatively stable in the following years. This phenomenon may be attributed to the increase in the number of supraglacial lakes due to the rise in Arctic temperatures from 2019 to 2020 (Zheng et al., 2023). In subsequent years, the water depth remained relatively stable (Figure 6 (b)-(e)). Besides, Figure 8 shows the changes in lake volume from 2019 to 2023. There was significant growth in lake volume in 2020 compared to the same period in 2019. However, the lake depth remained relatively consistent from 2020 to 2023. The changes in lake volume during the same period in different years may be related to global warming.

5.3 Limitations of the method

This polar SDB method based on Sentinel-2 and ICESat-2 has some limitations. The availability of high-quality ICESat-2 data that passes over supraglacial lakes is limited, which significantly restricts the accuracy of bathymetric inversion and the applicability of the inversion model. Occasional occurrences of anomalous water depth values are observed, and the direct transferability of the bathymetric inversion model to different years is challenging. As a result, when ICESat-2 data was lacking before 2018, the SDB method in this study could not be used to detect water depth changes, thus limiting the extension of water

depth detection to longer time series. Although ArcticDEM data offers high spatial resolution, its suitability for long-term inversion is also limited. Furthermore, the utilization of ArcticDEM is constrained by the reliance on the surface photon elevations of ICESat-2 data as a reference, making it suitable only as validation data within an acceptable margin of error rather than as training data for water depth inversion. Therefore, the proposed method also requires an adequate number of ICESat-2 bathymetric photons to achieve satisfactory detecting results.

6. Conclusion

This study utilized Sentinel-2 and ICESat-2 data to derive bathymetry of supraglacial lakes in the southwest of Greenland from 2019 to 2023. The study also aims to compare the performance of three different SDB models in deriving bathymetry and detecting changes in lake volume over a long period. Using the log-linear model, log-ratio model, and BP neural network model, the bathymetry of the supraglacial lakes in the study regions was conducted and validated using high spatial resolution ArcticDEM. Results indicate that the log-ratio model demonstrated effectiveness in bathymetry inversion considering both inversion accuracy and efficiency. The R^2, RMSE, and MAE are 0.92, 0.79 m, and 0.62 m, respectively. In contrast, the log-linear model exhibited larger errors in bathymetry in deeper regions. Additionally, due to limited ICESat-2 data available for long-term bathymetry across supraglacial lakes and certain restrictions on the training samples for the BP neural network, errors in the mapping relationship were inevitable during bathymetry in some areas. The bathymetry results over the past five years indicate a general upward trend of supraglacial lake volume in the southwest lakes of GrIS with a relatively large increase from 2019 to 2020 and subsequent years show slight increments but overall remain stable. The volume changes during the same period of the past 5 years may be related to the concurrent change in temperatures caused by global climate warming which warrants concerns and further research. In summary, this study provides an SDB method for long-term inversion of Arctic supraglacial lake water depth, addressing the challenge of obtaining *in-situ* water depth data in Arctic regions. It also contributes to a deeper understanding of polar supraglacial lakes and serves as a reference for global climate change.

Acknowledgments

We would like to thank the anonymous reviewers for their comments and their insightful suggestions significantly improved this paper. This work was supported by the National Natural Science Foundation of China (42304051). We also thank the NASA, NOAA, ESA, and Polar Geospatial Center for providing data.

References

Albright, A., & Glennie, C. (2020). Nearshore bathymetry from fusion of Sentinel-2 and ICESat-2 observations. *IEEE Geoscience and Remote Sensing Letters*, *18*(5), 900-904.

Bin, C., Zhenge, Q., & Bincai, C. (2016). Comparison among four inverse algorithms of water depth [J]. *Journal of Geomatics Science and Technology*, *33*(04), 388-393.

Box, J. E., Hubbard, A., Bahr, D. B., Colgan, W. T., Fettweis, X., Mankoff, K. D., ... & Fausto, R. S. (2022). Greenland ice sheet climate disequilibrium and committed sea-level rise. *Nature Climate Change*, *12*(9), 808-813.

Duplančić Leder, T., Leder, N., & Peroš, J. (2019). Satellite derived bathymetry survey method–Example of Hramina bay. *Transactions on Maritime Science*, *8*(01), 99-108.

Fricker, H. A., Arndt, P., Brunt, K. M., Datta, R. T., Fair, Z., Jasinski, M. F., ... & Wouters, B. (2021). ICESat-2 meltwater depth estimates: application to surface melt on amery ice shelf, East Antarctica. *Geophysical Research Letters*, *48*(8), e2020GL090550.

Guo, X., Jin, X., & Jin, S. (2022). Shallow water bathymetry mapping from ICESat-2 and Sentinel-2 based on BP neural network model. *Water*, *14*(23), 3862.

He, J., Zhang, S., Feng, W., & Lin, J. (2024). Quantifying earthquake-induced bathymetric changes in a tufa lake using high-resolution remote sensing data. *International Journal of Applied Earth Observation and Geoinformation*, *127*, 103680.

Le Quilleuc, A., Collin, A., Jasinski, M. F., & Devillers, R. (2021). Very high-resolution satellite-derived bathymetry and habitat mapping using pleiades-1 and ICESat-2. *Remote Sensing*, *14*(1), 133.

Li, S., Su, D., Yang, F., Zhang, H., Wang, X., & Guo, Y. (2022). Bathymetric LiDAR and multibeam echo-sounding data registration methodology employing a point cloud model. *Applied Ocean Research*, *123*, 103147.

Li, S., Wang, X. H., Ma, Y., & Yang, F. (2023). Satellite-derived bathymetry with sediment classification using ICESat-2 and multispectral imagery: case studies in the South China Sea and Australia. *Remote Sensing*, *15*(4), 1026.

Liu, D., Chen, S., Liu, Q., Ke, J., Wang, N., Sun, Y., ... & Tao, Y. (2022). Spaceborne environmental detection lidar and its key techniques. *Acta Opt. Sin*, *42*, 1701001.

Lyzenga, D. R. (1978). Passive remote sensing techniques for mapping water depth and bottom features. *Applied optics*, *17*(3), 379-383.

Lyzenga, D. R. (1985). Shallow-water bathymetry using combined lidar and passive multispectral scanner data. *International journal of remote sensing*, *6*(1), 115-125.

Ma, Y., Xu, N., Liu, Z., Yang, B., Yang, F., Wang, X. H., & Li, S. (2020). Satellite-derived bathymetry using the ICESat-2 lidar and Sentinel-2 imagery datasets. *Remote Sensing of Environment*, *250*, 112047.

McFeeters, S. K. (1996). The use of the Normalized Difference Water Index (NDWI) in the delineation of open water features. *International journal of remote sensing*, *17*(7), 1425-1432.

Melling, L., Leeson, A., McMillan, M., Maddalena, J., Bowling, J., Glen, E., ... & Lørup Arildsen, R. (2023). Evaluation of satellite methods for estimating supraglacial lake depth in southwest Greenland. *The Cryosphere Discussions*, *2023*, 1-28.

Morin, P., Porter, C., Cloutier, M., Howat, I., Noh, M. J., Willis, M., ... & Peterman, K. (2016, April). ArcticDEM; a publically available, high resolution elevation model of the Arctic. In *Egu general assembly conference abstracts* (pp. EPSC2016-8396).

Moussavi, M. S., Abdalati, W., Pope, A., Scambos, T., Tedesco, M., MacFerrin, M., & Grigsby, S. (2016). Derivation and validation of supraglacial lake volumes on the Greenland Ice Sheet from high-resolution satellite imagery. *Remote sensing of environment*, *183*, 294-303.

Parrish, C. E., Magruder, L. A., Neuenschwander, A. L., Forfinski-Sarkozi, N., Alonzo, M., & Jasinski, M. (2019). Validation of ICESat-2 ATLAS bathymetry and analysis of ATLAS’s bathymetric mapping performance. *Remote sensing*, *11*(14), 1634.

Stumpf, R. P., Holderied, K., & Sinclair, M. (2003). Determination of water depth with high-resolution satellite imagery over variable bottom types. *Limnology and Oceanography*, *48*(1part2), 547-556.

Thomas, N., Pertiwi, A. P., Traganos, D., Lagomasino, D., Poursanidis, D., Moreno, S., & Fatoyinbo, L. (2021). Space-borne cloud-native satellite-derived bathymetry (SDB) models using ICESat-2 and Sentinel-2. *Geophysical Research Letters*, *48*(6), e2020GL092170.

Zhang, X., Ma, Y., Li, Z., & Zhang, J. (2022). Satellite derived bathymetry based on ICESat-2 diffuse attenuation signal without prior information. *International Journal of Applied Earth Observation and Geoinformation*, *113*, 102993.

ZHAO, H., XU, X., & WU, Y. (2001). Perspective of development of multibeam swath techniques. *Journal of harbin engineering university*, *22*(2), 41-45.

Zheng, L., Li, L., Chen, Z., He, Y., Mo, L., Chen, D., ... & Cheng, X. (2023). Multi-sensor imaging of winter buried lakes in the Greenland Ice Sheet. *Remote Sensing of Environment*, *295*, 113688.

Zheng, L., Xia, L., & Jigang, Q. (2012). Polar Lake Ba-thymetry Retrieval from Remote Sensing Data of the Arctic Coastal Plain in Alaska. *Acta Scientia~ rum Naturalium Universitis Sunyatseni*, *51*(3), 128-134.